Towards Novel Multifunctional Pillared Nanostructures: Effective Intercalation of Adamantylamine in Graphene Oxide and Smectite Clays

Konstantinos Spyrou, Georgia Potsi, Evmorfia K. Diamanti, Xiaoxing Ke, Eleni Serestatidou, Ioannis I. Verginadis, Anastasia P. Velalopoulou, Angelos M. Evangelou, Yiannis Deligiannakis, Gustaaf Van Tendeloo, Dimitrios Gournis, and Petra Rudolf**

Multifunctional pillared materials are synthesized by the intercalation of cage-shaped adamantylamine (ADMA) molecules into the interlayer space of graphite oxide (GO) and aluminosilicate clays. The physicochemical and structural properties of these hybrids, determined by X-ray diffraction (XRD), Fourier transform infrared (FTIR), Raman and X-ray photoemission (XPS) spectroscopies and transmission electron microscopy (TEM) show that they can serve as tunable hydrophobic/hydrophilic and stereospecific nanotemplates. Thus, in ADMA-pillared clay hybrids, the phyllomorphous clay provides a hydrophilic nanoenvironment where the local hydrophobicity is modulated by the presence of ADMA moieties. On the other hand, in the ADMA-GO hybrid, both the aromatic rings of GO sheets and the ADMA molecules define a hydrophobic nanoenvironment where sp^3-oxo moieties (epoxy, hydroxyl and carboxyl groups), present on GO, modulate hydrophilicity. As test applications, these pillared nanostructures are capable of selective/stereospecific trapping of small chlorophenols or can act as cytotoxic agents.

1. Introduction

Diamondoids have been extensively studied in recent years due to their successful application in diverse fields of nano- and biotechnology[1] which rely on the physical and chemical properties[2] imparted by their unique (cage-like) structure of tricyclic saturated hydrocarbons. Applications reported in the literature for these "molecular diamonds" include their use as templates in nanotechnology, or as molecular building blocks for the synthesis of novel catalysts,[3] high temperature polymers,[4] or hybrid nanostructures.[5] In the pharmaceutical industry diamondoids are employed in drug delivery and as drug targeting agents,[6] as well as in antiviral drugs (influenza A)[7] and in the treatment of Parkinson's and Alzheimer's.[8] To further extend the use of diamandoids, host/guest chemistry can help to tune or protect the properties of these molecules. In this context, adamantylamine (ADMA), a derivative of the smallest diamondoid, adamantane, with a covalently attached amino group, is expected to be an ideal pillaring block to be incorporated in layered host materials such as aluminosilicate clays or graphene oxide (GO), giving rise to new hybrid multifunctional nanostructures.

Layered materials represent a diverse and largely untapped source of 2D nanosystems with high specific surface area and exceptional physicochemical properties that are important for applications such as catalysis, sensing, environmental remediation, biotechnology, and energy storage.[9] The nature of the environment between the 2D nanometer-sized sheets regulates the topology of the intercalated molecules and affects possible supramolecular rearrangements or reactions, such as self-assembling processes that are usually not easily controlled in solution.[10] Smectite clays and graphene oxide are two archetypical layered materials; smectite clays are minerals consisting of aluminosilicate nanoplatelets, with a unique combination of swelling, intercalation and ion exchange properties that make them valuable nanostructures[11] for use as catalysts,[12] templates in organic synthesis,[13] building blocks

Dr. K. Spyrou, Prof. P. Rudolf
Zernike Institute for Advanced Materials
University of Groningen
Nijenborgh 4 NL-9747AG, Groningen, The Netherlands
E-mail: p.rudolf@rug.nl

G. Potsi, Dr. E. K. Diamanti, Prof. D. Gournis
Department of Material Science and Engineering
University of Ioannina
GR-45110, Ioannina, Greece
E-mail: dgourni@cc.uoi.gr

Dr. X. Ke, Prof. G. V. Tendeloo
EMAT (Electron Microscopy for Materials Science)
University of Antwerp
Groenenborgerlaan 171 B-2020, Antwerpen, Belgium

E. Serestatidou, Prof. Y. Deligiannakis
Department of Environmental and
Natural Resources Management
University of Western Greece
Seferi 2 GR-30100, Agrinio, Greece

Dr. I. I. Verginadis, Dr. A. P. Velalopoulou,
Prof. A. M. Evangelou
Laboratory of Physiology
Faculty of Medicine, University of Ioannina
GR-45110, Ioannina, Greece

DOI: 10.1002/adfm.201400975

for composite materials,[10a,14] adsorbents of inorganic and/or organic pollutants,[15] as active agents or excipients of medicinal products[16] and as constituents of modified drug delivery systems (MDDS)[17] in pharmaceutical industry. In most cases, the intercalation process is a simple ion-exchange procedure between hydrated cations present in the galleries of the clay and organic or inorganic cation moieties. Unlike the intercalation of graphite, that of smectite clays does not necessarily involve charge transfer between the host and the guest species. On the other hand, graphite oxide (GO) is an oxygen rich derivative of graphite decorated with hydroxyl, epoxy, and carboxyl groups (sp^3-oxo moieties).[18] These functional groups are created by strong oxidation and distributed randomly on the basal planes and edges of the GO sheets, generating aliphatic regions (sp^3-carbon atoms) within the sp^2-hybrized matrix. Due to the existence of such hydrophilic moieties, GO presents similar properties as smectite clays in that it is prone to swelling and intercalation. Both GO and intercalated GO are being considered for numerous applications such as supercapacitors,[19] high mobility transistors,[20] lithium batteries,[21] hydrogen storage, adsorption of organic moieties[22] or the removal of pollutants (e.g. chlorophenols) from aqueous solutions; recently they have also attracted interest regarding their potential use in biomedical applications. GO has already been studied in drug delivery formulation and bioanalysis[23] as well as for its potential cytotoxic action.[24] In contrast to clays, the intercalation process of GO involves covalent bonding of guest molecules to the oxygen-containing groups on the GO surfaces (nucleophilic substitution reactions). It has been demonstrated that, under proper conditions, GO can be exfoliated in water forming colloidal suspensions of single graphene oxide sheets.[25]

In this work, we report on the intercalation of adamantylamine (ADMA) into two types of layered matrices, graphene oxide and smectite clay. Apart from the different structural and geometrical characteristics (e.g. interlamellar space) that might occur using different matrices, and which in turn define the stereospecific properties of the final pillared structures, the choice of these two 2D nanotemplates was also motivated by their ability to provide, in conjunction with the adamantane moieties, diverse tunable hydrophobic or hydrophilic character (environment) in the final hybrids. Thus, in the ADMA-clay hybrids, smectite clay provides a hydrophilic nanoenvironment where local hydrophobicity is modulated by the presence of ADMA moieties, while in the ADMA-GO hybrid, both the aromatic rings of GO sheets and the ADMA molecules define a hydrophobic nanoenvironment, where oxygen-containing groups present on GO modulate the hydrophilicity. Since the incorporation of ADMA into these layered materials opens the way to diverse applications in the chemical, pharmaceutical and electronic (sensor) industry, we decided to perform also two representative case studies of great importance in biomedicine and environmental remediation, namely the use of these hybrid nanostructures as antiproliferative agents in cells and as effective adsorbents for the removal of organic pollutants from aqueous solution.

2. Results and Discussion

Smectite clay consists of octahedral alumina layers, each fused between two tetrahedral silica layers. In the tetrahedral sheet

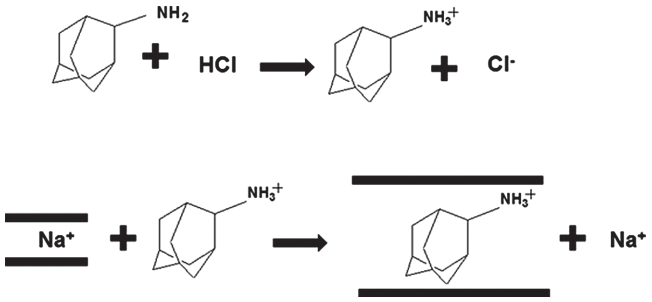

Scheme 1. Schematic representation of the intercalation process of adamantylamine (ADMA), after the protonation of the amine end groups, into the inter-lamellar space of clay. The bold lines represent the negatively charged clay platelets.

Al^{+3} can replace Si^{+4} creating a negative charge. Occasionally Fe^{+3} cations are also present in the tetrahedral lattice. In the octahedral sheets negative charging may occur by substitution of Mg^{+2} for Al^{+3} while Fe^{+2} and Fe^{+3} may also part of the octahedral sheets. The negative charge of the isomorphous substituents is compensated by hydrated cations (usually sodium) present in the interlayer space. These charge balancing cations can be replaced with water soluble organic or inorganic cationic species;[11] this approach was followed to intercalate ADMA in two different clay minerals, namely SWy-2 montmorillonite (product called SWy-2/ADMA in the following) and a synthetic trioctahedral hectorite, Laponite RD (product called Lap/ADMA). Initially the terminal amine groups of adamantylamine had to be protonated to form a cationic adamantane species. The intercalation of the positively charged adamantylamine, readily dispersed in aqueous solution, was achieved by ion-exchange according to the reaction (**Scheme 1**):

Contrary to clay minerals, GO does not contain charge balancing cations, thus intercalation is obtained by grafting to functional groups on the GO surface and/or adsorption of molecules held between the basal planes by van der Waals interactions. ADMA was intercalated in oxidized graphite as sketched in **Scheme 2**; the product is called GO/ADMA in the following. When ADMA, dissolved in distilled deionized water, was added to a water dispersion of GO, an immediate flocculation of GO particles was observed. This phenomenon is induced by the insertion of adamantylamine in the GO galleries through covalent bonding via the amine functionality of the adamantane derivative (see X-ray photoelectron spectroscopy data below). The amine end groups interact via a ring opening reaction of the epoxide groups of GO.[25,26]

The success of the intercalation reaction can be proven by X-ray diffraction (XRD) which allows estimating the interlayer spacing between GO or clay sheets. The XRD patterns of GO/ADMA and SWy-2/ADMA are displayed in **Figure 1**. The insertion of adamantylamine between the aluminosilicate and graphene oxide layers increases the interlayer distance. More specifically, for intercalation in SWy-2 clay, the basal d_{001}-spacing, which is 12.4±0.3 Å in the initial montmorillonite clay, becomes 15.6 Å after the modification; this corresponds to an interlayer separation of 15.6–9.6 = 6 Å, where 9.6 Å represents the thickness of a clay layer.[10d] This value is in accordance with the size of the adamantylamine molecule if we assume an orientation perpendicular to the aluminosilicate platelets.[27] In the case of

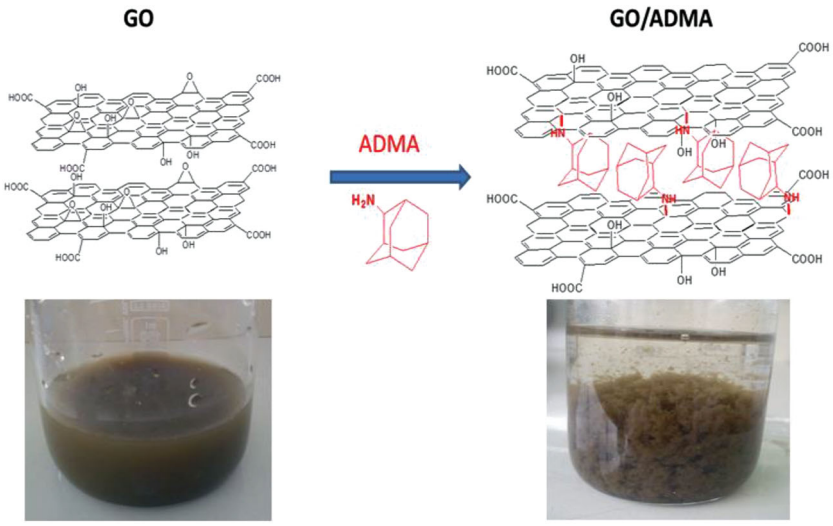

Scheme 2. Schematic representation of the synthetic procedure of GO/ADMA.

GO/ADMA, the 001 diffraction peak centered at ~12° in pristine GO shifts to lower angles corresponding to a d_{001}-spacing of 10.4±0.3 Å. Taking into account the thickness of a graphene oxide layer (6.1 Å),[28] this corresponds to an interlayer separation of Δ = 10.4 – 6.1 = 4.3 Å occupied by the ADMA pillaring moieties. This value implies that the adamantane derivative must adopt an inclined orientation in the GO interlayer space.[29]

An additional tool for the characterization of hybrid pillared materials is Fourier transform infrared (FTIR) spectroscopy, which can confirm the successful incorporation of the adamantane derivative in the layered matrices. **Figure 2** displays the FTIR spectra of SWy-2 and GO before and after the intercalation process. In the case of SWy-2/ADMA, the spectrum displays all the characteristic bands arising from aluminosilicate clay at 465 cm^{-1} (Si–O–Si and Si–O bending vibrations), 524 cm^{-1} (Si–O–Si bending), 778 cm^{-1} (Si–O deformation), 797 cm^{-1} (Si–O and Si–O–Al stretching), 884 cm^{-1} (Al–Fe–OH deformation), 918 cm^{-1} (Al–OH–Al bending), 1047 cm^{-1} (Si–O–Si stretching) and 1639 cm^{-1} (H_2O bending).[30] In addition, the presence of adamantylamine in the hybrid material is revealed by the bands centered at 2863 cm^{-1} and 2921 cm^{-1} corresponding to stretching vibrations of C–H, as well as by the peak at 1520 cm^{-1}, due to N–H vibrations.[10c,31] In the

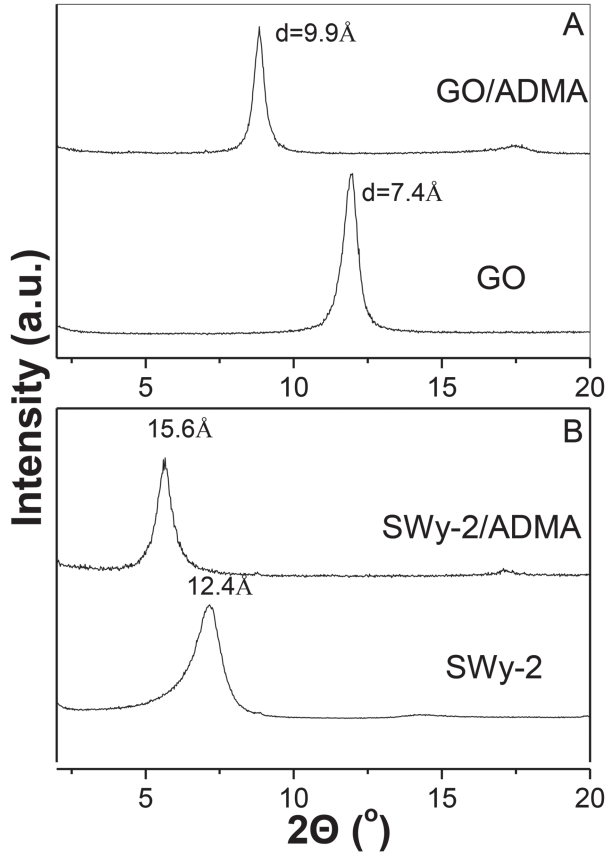

Figure 1. Comparison of the X-ray diffraction patterns of the hybrid pillared systems A) SWy-2/ADMA and B) GO/ADMA with those of the pristine layered matrices (SWy-2 and GO).

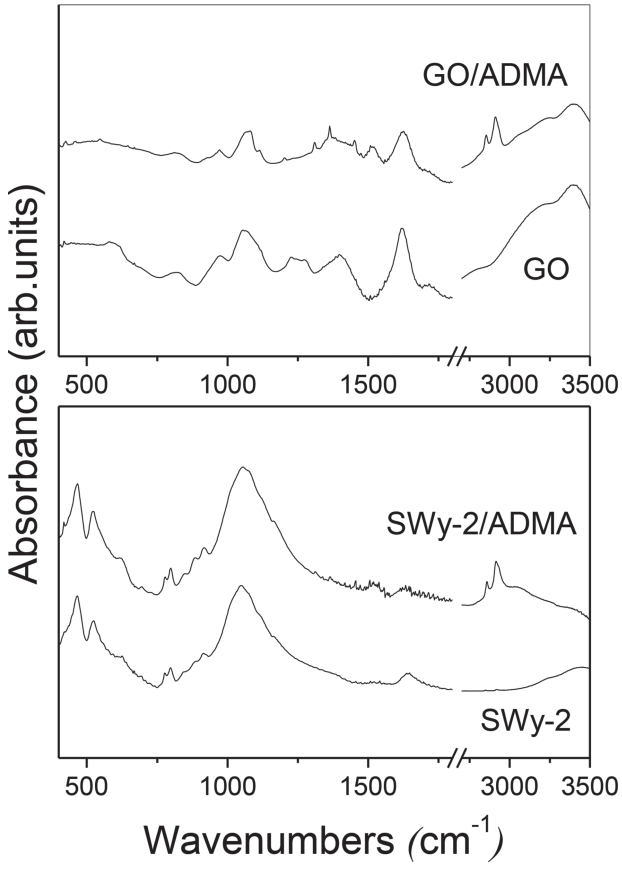

Figure 2. FTIR spectra of the hybrid pillared systems SWy-2/ADMA and GO/ADMA; the FTIR spectra of pristine SWy-2 and GO are plotted for comparison.

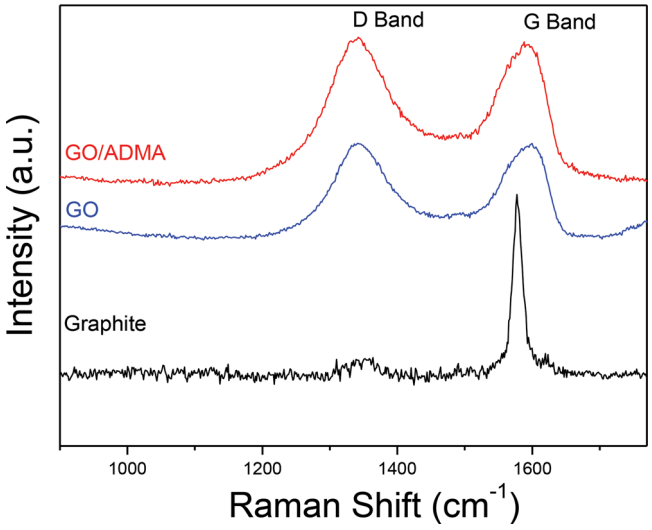

Figure 3. Raman spectra of pristine graphite, GO and GO/ADMA excited at 532 nm.

case of GO/ADMA the same peaks originating from the ADMA molecules are also present in the spectrum, together with characteristic bands arising from GO at 3410 cm^{-1} (hydroxyl stretching vibration of C–OH groups), 1621 cm^{-1} (C=O stretching vibrations of the –COOH groups), 1396 cm^{-1} (O–H deformations of the C–OH groups) and 1062 cm^{-1} (C–O stretching vibrations).[32]

In the case of GO/ADMA Raman measurements were performed as well (see **Figure 3**). Raman spectroscopy is a widely used in the characterization of carbon-based materials because it provides information about their structure. The Raman spectrum of the graphite used as starting material includes the G peak at approximately ~1580 cm^{-1}, as well a very weak 2D band located at ~1353 cm^{-1}, caused by the tangential E_{2g} in-plane vibration mode of the graphite lattice and second order boundary phonons (A_{1g} breathing mode) respectively.[33] The 2D band is associated with defects leading to sp^3 carbon atoms.[34] The GO sample exhibits strong fluorescence and therefore its week Raman spectrum could not be observed when exciting at 532 nm. To overcome this problem, a sample obtained by deposition of GO sheets on a gold substrate, as described elsewhere,[25b] was used. After the chemical oxidation of graphite the G band is broadened and shifted slightly to 1594 cm^{-1}, while the D band at 1363 cm^{-1} becomes prominent due to defects created by the attachment of oxygen-containing groups (sp^3-oxo moieties) to the carbon basal planes.[35] The degree of disorder in the carbon flakes can be expressed by the ratio between intensities of the G and D bands. In the case of GO, the I_D/I_G ratio is 1.06 pointing to the creation of sp^3 domains in the oxidation treatment. After the intercalation of the organic moieties that ratio remains almost the same. This gives further support to the covalent bonding of the adamantane derivatives to the epoxy groups on the GO surface since such a bonding does not decrease the number of aromatic carbon-carbon bonds.

To verify the presence and integrity of the adamantylamine cycloalkanes within the layered nanostructures, as well as to analyse the chemical environment of ADMA, we employed X-ray photoelectron spectroscopy (XPS). The XPS spectrum

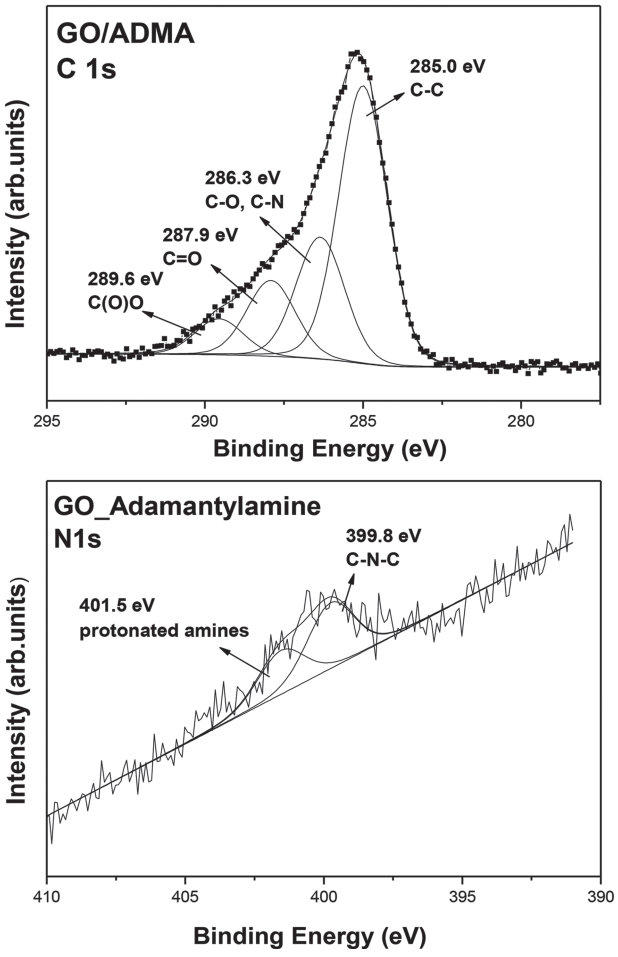

Figure 4. XPS spectra of the C1s (top) and N1s (bottom) core level regions of the GO/ADMA hybrid.

of GO/ADMA reveals in C1s core level region (**Figure 4** top) the characteristic contribution of C–C/C–H bonds of the GO lattice and of the adamantane cyclohexane ring centered at a binding energy of 285.0 eV; these bonds contribute 54.3% of the total carbon 1s intensity. The peak at 286.3 eV is due to C–O/C–N bonds and represents 23.8% of the total carbon 1s intensity. Finally two components at 287.9 eV and 289.6 eV are attributed to carbonyl (C=O) and carboxyl (O–C=O) groups respectively, which are created on the basal planes and at the boarders of the carbon sheets by the acid treatment. The N1s core level region of the XPS spectrum of GO/ADMA, plotted in Figure 4 (bottom), exhibits two main peaks, located at 399.8 eV and 401.5 eV. They arise from the amine end groups of ADMA chemically grafted to the epoxy groups of GO,[36] and from protonated amines ionically bonded to the carboxylic acid anionic groups of GO,[37] respectively (for comparison the corresponding XPS spectrum of pristine ADMA is presented in the Supporting Information, Figure S3).

XPS measurements were also performed for the SWy-2/ADMA hybrid system. The survey spectra of SWy-2 and SWy-2/ADMA are shown in the supporting information, Figure S4. Characteristic photoelectron and Auger peaks of O, Si, Al, and Mg are clearly distinguishable in the spectrum of pristine

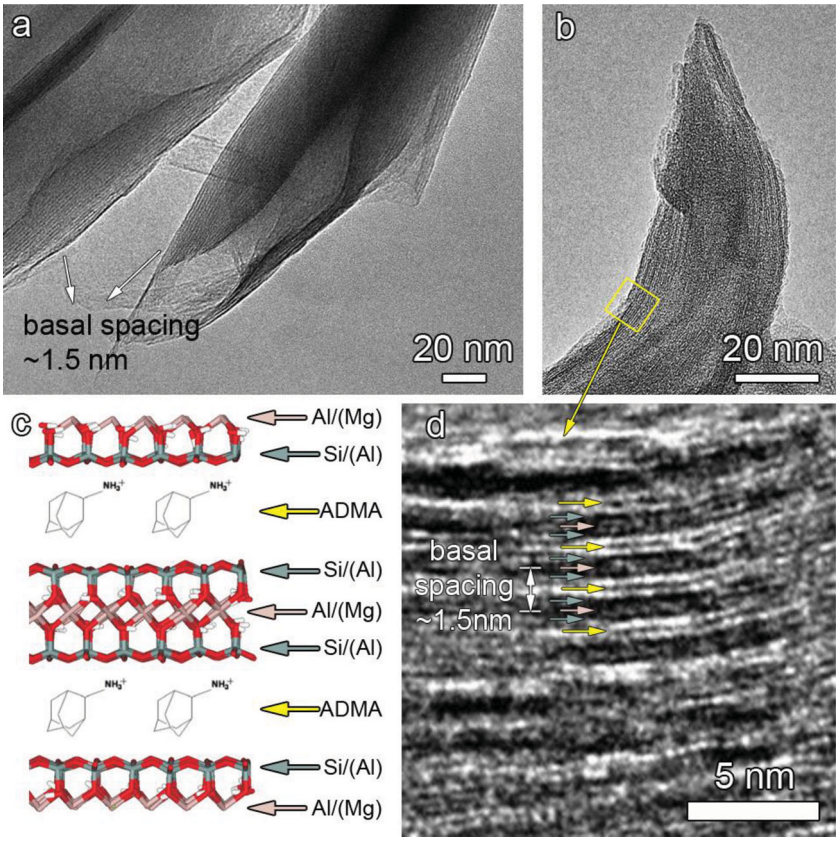

Figure 5. a) TEM image of ADMA-intercalated SWy-2 at low magnification. The basal spacing is measured to be approximately 1.5 nm, consistent with the XRD measurement. b) TEM image at higher magnification, with a zoomed-in image shown in (d). The intercalated ADMA layer (indicated by yellow arrows) can be recognized between clay layers which are composed c) of an octahedral layer (pink arrow) sandwiched between two tetrahedral layers (blue arrows).

montmorillonite clay. A small carbon peak appears, mainly due to adventitious carbon always present on the outer surface of air-exposed[38] materials but also due to soil organic matter present in natural clay minerals.[38a,39] After the insertion of ADMA a pronounced increase in the intensity of the carbon signal points to the presence of adamantylamine inside the clay galleries. Quantitatively, the incorporation of ADMA in the clay is determined by measuring the ratio between the carbon 1s and the silicon 2p core level photoemission intensities before and after the intercalation process (see Supporting Information Figure S5). The C1s/Si2p intensity ratio increased from 1.42 ± 0.06 before the incorporation of adamantylamine to 2.79 ± 0.11 after the introduction of ADMA. The presence of the amine terminal groups on adamantane is deduced from the N1s photoelectron spectrum (see Supporting Information, Figure S6).

Undeniable proof for the successful intercalation of ADMA in the interlayer space of montmorillonite clay comes from the high-resolution transmission electron microscopy (HRTEM) investigation, as shown in **Figure 5**. From the TEM image of ADMA-intercalated SWy-2 at low magnification (Figure 5a) the interlayer separation can be estimated, while the high degree of stacking of the clay platelets is also confirmed. The basal spacing is measured to be ~1.5 nm, in agreement with the XRD findings. Moreover, in the HRTEM image at higher magnification shown in Figure 5b, as well as in the zoomed-in image shown in Figure 5d, intercalated ADMA layers (indicated by yellow arrows) can be recognized between clay layers; the latter are composed of an octahedral layer (pink arrow) sandwiched between two tetrahedral layers (blue arrows) as expected for a 2:1 layered silicate like montmorillonite where an octahedral alumina layer is fused between two tetrahedral silica layers.

To estimate the amount of admantylamine introduced in GO and in clay, thermogravimetric analysis (TGA) and differential thermal analysis (DTA) measurements were performed (see Supporting Information, Figures S6 and S7) on two pillared hybrids (GO/ADMA and SWy-2/ADMA) as well as on the pristine materials. Based on these data, the weight loss observed in the temperature range 280–400 °C originates from the combustion of the amino groups of adamantylamine[40] and is calculated to be equal to 8 and 4 wt% for GO/ADMA and SWy-2/ADMA, respectively. Moreover, in the case of SWy-2/ADMA, between 400 °C and 700 °C another weight loss of 8.5 wt% is observed, which is due to combustion of the cycloalkane of adamantylamine. Based on the latter two weight losses, we estimate that the amount of intercalated adamantylamine in the SWy-2/ADMA hybrid material corresponds to ~12.5 wt% of the total mass. In the case of GO/ADMA the second weight loss cannot be distinguished from the combustion of the graphene oxide layers which takes place in this same temperature range.

Nitrogen adsorption-desorption measurements (at 77 K) were performed on both GO/ADMA and SWy-2/ADMA in order to reveal the creation of pillared structures. **Table 1** reports the specific-surface-areas obtained through BET analysis (S_{BET}) for the pristine layered matrices, GO and SWy-2, and for the corresponding pillared hybrid nanostructures. The specific surface area of pure GO (~9 $m^2 g^{-1}$) is small indicating that N_2 can only adsorb on the external surfaces of GO and reduced GO while the interlayer space of GO is inaccessible. However, for the GO/ADMA hybrid the specific surface area is four times higher (37 $m^2 g^{-1}$) than for GO, supporting the hypothesis that

Table 1. Specific surface area values for GO and SWy-2 and final hybrids GO/ADMA and SWy-2/ADMA

	Specific Surface Area (S_{BET}) [$m^2 g^{-1}$]
GO	9
GO/ADMA	37
SWy-2	65
SWy-2/ADMA	135

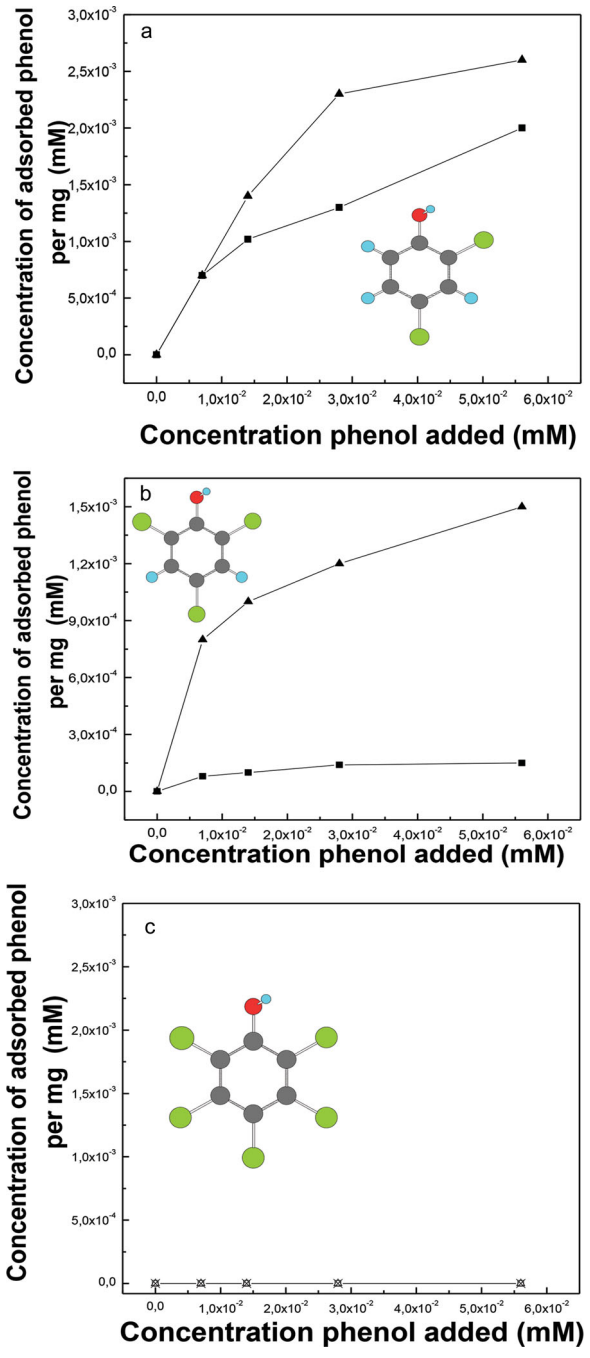

Figure 6. (A) Langmuir adsorption isotherms of 2,4-DCP on pristine SWy-2 clay (■) and SWy-2/ADMA (▲), (B) Adsorption isotherms of 2,4,6-TCP on pristine SWy-2 clay (□) and SWy-2/ADMA (△), (C) Adsorption isotherms of PCP on pristine SWy-2 clay (⊠) and SWy-2/ADMA (⊠).

adamantylamine acts as pillaring species. In fact, this result implies that nitrogen adsorbs not only on the external surface but also in the pores between the ADMA pillars. The results were more pronounced in the case of the montmorillonite hybrid which showed a significantly increased BET surface area (135 $m^2 g^{-1}$) compared to pristine montmorillonite clay.

In view of possible applications for these new pillared hybrids, we tested whether SWy-2/ADMA and GO/ADMA are capable of adsorbing organic pollutants (phenol derivatives) from solution. In **Figure 6** the adsorption isotherms of 2.4.6-trichlorophenol (TCP), 2.4-dichlorophenol (DCP) and pentachlorophenol (PCP), in the starting material (SWy-2) and in the SWY-2/ADMA hybrid are shown. The adsorption isotherms show a plateau at increased chlorophenol:clay ratios which defines the maximum adsorption capacity of the material, listed in **Table 2**. As evident from the isotherms, TCP and DCP phenols adsorb in the interlayer space of the pristine clay as well as in the pores of SWy-2/ADMA, while the adsorption of PCP remained zero in all cases. From Table 2 one notices that the adsorption of the various phenols followed a consistent trend for all materials.

The uptake of DCP was significantly higher than that of TCP. Strikingly the adsorption of PCP remained zero in all cases; the adamantylamine -intercalated clay showed an improved adsorption capacity with respect to the pristine one. Indeed, SWy-2/ADMA adsorbed significantly higher amounts of DCP for all concentrations of added phenol and showed a 40% enhanced uptake compared to the pristine clay at the highest phenol concentrations, see Table 2. SWy-2/ADMA also adsorbed almost eight times more TCP than the SWy-2. Comparing the three types of chlorophenols we conclude that the higher adsorption of DCP than of TCP as well as the negligible adsorption of PCP could be explained by the molecular size of the three phenols (stereospecific trapping): TCP and PCP are larger, so they might block the pores of the pillared hybrid and thereby hamper the adsorption of further molecules (see physical model below).

Figure 7 presents the adsorption isotherms for TCP, DCP and PCP by GO/ADMA and by pristine GO. GO appears to adsorb none of the chlorophenols, whereas GO/ADMA adsorbs selectively only DCP while the adsorption of TCP and of PCP was minimal.

The observed differences in the uptake of PCP, 2,4,6-TCP and 2,4-DCP can be attributed to the difference in the molecular size of the phenols. The molecular volumes are 60.3 $Å^3$ for DCP, 67.9 $Å^3$ for TCP and 83.2 $Å^3$ for PCP (see Supporting Information Table S1). Thus, the more bulky PCP is adsorbed less by the pillared clay and not at all by GO/ADMA, while DCP seems to be able to penetrate (stereospecific trapping) in the interlamellar space of both SWy-2/ADMA and GO/ADMA. This can be explained if we take into account the change in the interlamellar space as depicted in Figure 1. The interlayer distance of the pristine SWy-2 clay is 2.8 Å and becomes 6.0 Å in SWy-2/ADMA. On the other hand, the interlayer distance in pristine GO is 1.3 Å, which is much smaller than that of the pristine SWy-2 clay, and becomes 4.3 Å after modification with adamantylamine. Despite this increase, only DCP can be accommodated GO/ADMA and this results in the observed

Table 2. Maximum adsorption capacity for chlorophenol [mM per mg] by SWy-2 montmorillonite clay, GO and their derivatives SWy-2/ADMA and GO/ADMA.

Chlorophenol	SWy-2	SWy-2/ADMA	GO	GO/ADMA
2,4-DCP	20×10^{-4}	27×10^{-4}	0	32×10^{-4}
2,4,6-TCP	2×10^{-4}	15×10^{-4}	0	1.3×10^{-4}
PCP	0	0	0	0

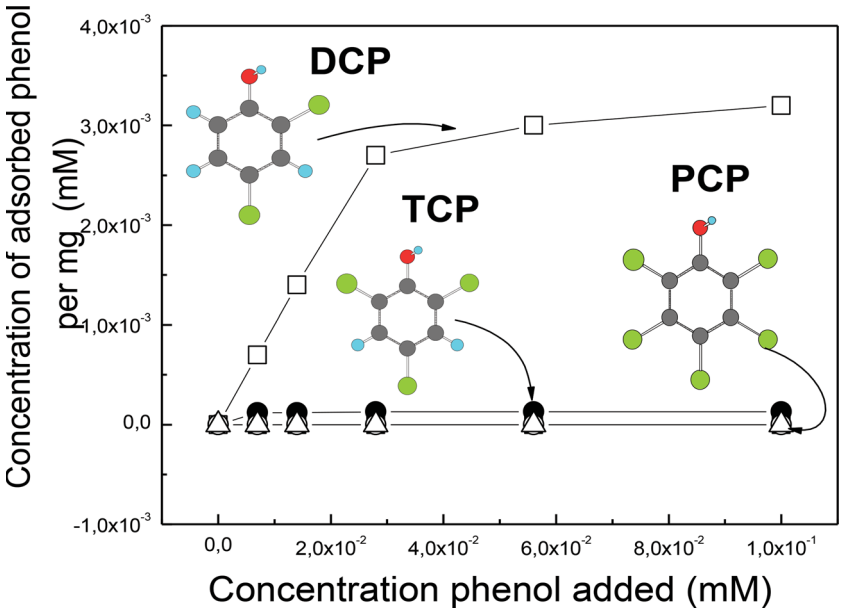

Figure 7. Adsorption isotherms of 2,4-DCP on pristine GO (■) and on GO/ADMA (□); of 2,4,6-TCP on pristine GO (○) and on GO/ADMA (l); of PCP on pristine GO (△) and on GO/ADMA(▲).

significant adsorption of DCP in contrast to TCP and PCP (selective/stereospecific adsorption).

Another possible future application of the pillared layered nanostructures is their use as potent cytotoxic agents. We chose laponite and intercalated laponite for these tests because this synthetic clay with small platelet size is used in pharmaceutical industry as drug carrier[41] (a detailed characterization of Lap/ADMA hybrid is presented in Supporting Information). Nevertheless, there is a gap in knowledge concerning Laponite's in vitro antiproliferative activity. Thus, the present study evaluated the in vitro cytotoxic activity of adamantylamine, laponite and of the intercalated laponite, Lap/ADMA, against a cancer cell line (A549) and a normal one (MRC-5). Parallel to Lap/ADMA we also tested the cytotoxic behavior of GO and GO/ADMA. The IC_{50} (μg mL^{-1}) values for cell proliferation (MTT assay) after 48 h of treatment with adamantane hybrids and pristine materials are shown in **Table 3** for A549 and MRC-5 cells and schematically presented in **Figure 8**. The IC_{50} values of ADMA, Lap and Lap/ADMA for A549 cells were 122 ± 13.7 μg mL^{-1}, 205 ± 20.7 μg mL^{-1} and 91 ± 5.0 μg mL^{-1}. It is noteworthy that Lap and Lap/ADMA exhibited cytotoxic activity on MRC-5 cells (normal cells) in concentration higher than 250 μg mL^{-1} (288 ± 41.8 μg mL^{-1} and 307 ± 32.2 μg/mL for Lap and Lap/ADMA, respectively). The IC_{50} (μg mL^{-1}) values for cell proliferation (MTT assay) after 48 h of treatment with GO and GO/ADMA for A549 cells were 259 ± 48 μg mL^{-1} and 192 ± 27.6 μg mL^{-1}, respectively, whereas GO and GO/ADMA exhibit cytotoxic action on normal cells (MRC-5) in concentration higher than 400 μg mL^{-1} (IC_{50} values for MRC-5 cells were 1480 ± 39.6 μg/mL and 425 ± 52.6 μg/mL for GO and GO/ADMA, respectively). What we observe is that Lap, Lap/ADMA, GO, GO/ADMA and ADMA exhibited antiproliferative activity against A549 cells. The control wells, containing different volumes of sterilized water (solvent) equal to volumes of the solutions added to the test wells, did not present any cytotoxicity against both cell lines (data not presented). All substances, except ADMA, exhibited a mild cytotoxic activity on MRC-5 cells, with IC_{50} values higher than 250 μg/mL and among all, Lap/ADMA is the most cytotoxic agent against the cancer cell line. In addition, Lap/ADMA showed a significantly higher cytotoxicity ($p < 0.05$) compared to that of laponite (starting material) and adamantylamine against A459 cells. Similarly there is a statistically significant difference between cell lines treated with GO and GO/ADMA ($p < 0.05$). Also GO/ADMA showed a lower cytotoxicity ($p < 0.05$) compared with GO.

Table 3. IC_{50} values (μg/mL) of ADMA, Lap, Lap/ADMA, GO and GO/ADMA on A459 and MRC-5 cells.

IC_{50} [μg/mL]	A549	MRC-5
ADMA	122 ± 13.7	149 ± 38.6
Lap	205 ± 20.7*	288 ± 41.8
Lap/ADMA	91 ± 5.0*,a	307 ± 32.2
GO	259 ± 48*	480 ± 39.6
GO/ADMA	192 ± 27.6*	425 ± 52.6

*Significant difference between cell lines; [a]Significant difference between Lap and Lap/ADMA; $p < 0.05$. Data are presented as mean ± σ (where σ is the standard deviation).

3. Conclusions

We successfully achieved the intercalation of adamantylamine into the interlayer space of layered host materials, namely

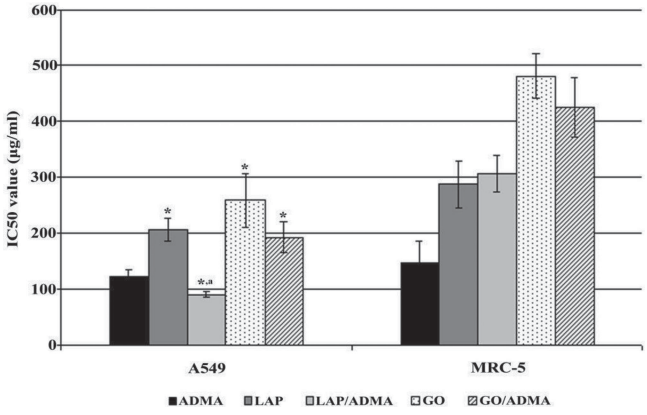

Figure 8. IC_{50} (μg/mL) values of ADMA, Lap/ADMA and GO/ADMA on A549 and MRC-5 cells, compared with pristine laponite clay (Lap) and GO.

graphite oxide, montmorillonite and laponite clay. X-ray diffraction measurements demonstrated the successful intercalation of adamantylamine into all three host matrixes. In the case of montmorillonite an undeniable proof for the successful intercalation was provided by transmission electron microscopy. X-ray photoelectron spectroscopy, FTIR spectroscopy as well as thermogravimetric and differential thermal analysis illustrated the type of interactions between the host materials and the intercalated molecules as well as informing on the intercalation yield. Porosimetry measurements revealed that pillared structures are created and gave the specific surface area of the hybrid nanostructures. The hybrid nanomaterial obtained by intercalation of adamantylamine into montmorillonite clay is capable of adsorbing significant quantities of organic pollutants which entails a significant potential for environmental remediation. GO/ADMA showed a stereospecificity-determined selective DCP uptake. Finally the hybrid nanostructures obtained by intercalation of adamantylamine into laponite clay and graphene oxide were investigated for their cytotoxicity against one cancer cell line and one normal cell line. The findings revealed that Lap/ADMA and GO/ADMA presented improved cytotoxic activity on A549 cells, whilst the cytotoxicity towards MRC-5 cells (normal cells) is maintained or only slightly increased as compared to Lap and GO, respectively. Possibly, the two components of the hybrid act synergistically by combining two different molecular pathways, leading to higher cytotoxicity. Further biological investigation is needed to elucidate the roles of Lap, GO, ADMA and their combinations on cancer and normal cell lines. We established a controllable and reproducible method for the synthesis of Multifunctional materials with potential for exploitation in the fields of environmental remediation and biomedical applications.

4. Experimental Section

Host Layered Materials: Graphene oxide was produced from graphite powder using a modified Staudenmaier's method.[25b,42] In a typical synthesis, 10 g of powdered graphite (purum, powder ≤0.2 mm; Fluka) were added to a mixture of concentrated sulphuric acid (400 mL, 95–97 wt%) and nitric acid (200 mL, 65 wt%) while cooling in an ice-water bath. Potassium chlorate powder (200 g, purum, >98.0%; Fluka) was added to the mixture in small portions while stirring and cooling. The reactions were quenched after 18 h by pouring the mixture into distilled water and the oxidation product washed until a pH 6. The sample, containing GO sheets of an average size of 5–10 μm,[25b] was then dried at room temperature. The clay used in this work was a natural Wyoming montmorillonite (SWy-2) obtained from the Source Clay Minerals Repository, University of Missouri, Columbia, with a cation exchange capacity (CEC) of 78 meq/100 g clay and particle size around 200 nm.[10c,43] The clay was fractionated to <2 μm by gravity sedimentation and purified by standard methods in clay science.[44] A sodium exchanged sample (Na^+-SWy-2) was prepared by immersing the clay in an aqueous solution of sodium chloride (1N). The cation exchange was completed by washing and centrifuging three times with the NaCl solution. The sample was finally washed with distilled deionized water and transferred into dialysis tubes in order to obtain chloride-free clay and then dried at room temperature. A synthetic trioctahedral hectorite, Laponite RD (Lap), produced by Laporte Industries Ltd., with structural formula $Na_{0.8}[Mg_{5.4}Li_{0.4}]Si_8O_{20}(OH)_4$, a CEC of 48.1 meq/100 g clay and an average particle size of 20 nm was used for the cytotoxic measurements.

Preparation of Clay/Adamantylamine Hybrid: 300 mg of Na^+-SWy-2 was dispersed upon vigorous stirring in 100 mL distilled deionized water and the system was stirred for 2 hours at room temperature. The dispersion was then reacted with 50 mg of 1-adamantylamine (97%, Aldrich) dissolved in 20/1 (v/v) ethanol/water. This amount corresponds to 1.5 times the CEC of SWy-2 montmorillonite. 5 drops of HCl 1M were then added and the mixture was stirred at room temperature for 24 hours. The residue was separated by centrifugation, washed three times with distilled deionized water and air-dried by spreading over a glass plate (product: **SWy-2/ADMA**). A similar procedure was used for the intercalation of ADMA (30 mg) in synthetic Laponite (sample: **Lap/ADMA**).

Preparation of Graphene Oxide/Adamantylamine Hybrid: In a typical experiment, 300 mg 1-adamantylamine were dissolved in ethanol (50 mL) and added dropwise to a dispersion of GO in distilled deionized water (100 mg GO in 50 mL) under vigorous stirring (pH = 8) at room temperature. Upon addition of adamantylamine the GO solid swelled instantly. The reaction continued for 24 h upon stirring at room temperature. The GO derivative was isolated by centrifugation and washed three times with 1:1 (v/v) ethanol/water and dried in air (sample denoted as **GO/ADMA**).

Characterization Techniques: The XRD patterns were collected on a D8 Advance Bruker diffractometer by using Cu Kα (40 kV, 40 mA) radiation and a secondary beam graphite monochromator. The patterns were recorded in the 2-theta (2Θ) range from 2 to 80°, in steps of 0.02° and a counting time of 2 s per step. Samples were in the form of films supported on glass substrates. For the preparation of the films, aqueous suspensions of the hybrids were deposited on glass plates and the solvent was allowed to evaporate slowly at ambient temperature. Infrared spectra were measured with a Perkin–Elmer Spectrum GX infrared spectrometer, in the region of 400–4000 cm^{-1}, equipped with a deuterated triglycine sulphate (DTGS) detector. Each spectrum was the average of 64 scans collected with 2 cm^{-1} resolution. Samples were in the form of KBr pellets containing ca. 2 wt% sample. Raman spectra were recorded with a Micro – Raman system RM 1000 RENISHAW, with excitation at 532 nm (Nd – YAG), in the range of 1000–2400 cm^{-1}. A power of 1 mW was used with a 1 μm focus spot in order to avoid photodecomposition of the samples. Thermogravimetric (TGA) and differential thermal (DTA) analysis were performed using a Perkin Elmer Pyris Diamond TG/DTA. Samples of approximately 5 mg were heated in air from 25 °C to 850 °C, at a rate of 5 °C min^{-1}. For the XPS measurements, 150 nm thick gold films supported on mica were used as substrates. All the samples were dispersed in distilled deionized water, and after stirring and sonication for 30 min, a small drop of the suspension was left to dry in air on the substrate. Samples were introduced via a load-lock system into a SSX-100 (Surface Science Instruments) photoelectron spectrometer with a monochromatic Al Kα X-ray source ($h\nu$ = 1486.6 eV). The base pressure in the spectrometer was 1×10^{-10} Torr during all measurements. The energy resolution was set to 1.16 eV in order to minimize the measuring time. The photoelectron take off angle was 37° with respect to the surface normal. An electron flood gun providing 0.3 eV kinetic energy electrons in combination with a gold grid mounted about 1 mm above the sample was used in the case of clays and clay hybrids to compensate for sample charging. All binding energies of GO and SWy-2 hybrids were referenced to the C1*s* core level of the C-C bond set to the nominal value of 285.0 eV,[45] while in the case of montmorillonite clays, all binding energies were referenced to the Si2p core level of smectite clay at 102.8 eV.[46] Spectral analysis included a Shirley background subtraction and peak deconvolution employing mixed Gaussian–Lorentzian functions, in a least squares curve-fitting program (WinSpec) developed at the LISE, University of Namur, Belgium. For the N1*s* line, however, a linear background subtraction was employed since the low peak intensity did not allow for a Shirley background subtraction. The nitrogen adsorption-desorption isotherms were measured at 77 K on a Sorptomatic 1990, Thermo Finnigan porosimeter. Specific surface areas were determined with the Brunauer-Emmett-Teller (BET) method using adsorption data points in the relative pressure P/P_0 range 0.01 to 0.30. High-resolution transmission electron microscopy (HRTEM)

data were collected using a FEI Tecnai G^2 microscope operated at 200 kV. TEM sample is prepared by dispersing the powder form of SWy-2/ADMA hybrid in ethanol before depositing onto a honeycomb carbon film supported by a copper grid.

Study of Cytotoxicity In Vitro: a) Cell lines and cell culture: Human lung cancer cells (A549) and normal human fetal lung fibroblasts (MRC-5) were kindly provided by Dr. Evangelos Kolettas, Laboratory of Physiology, Faculty of Medicine, University of Ioannina. All different cell lines were cultured in Dulbecco's Modified Eagles Medium (DMEM) enriched with 10% fetal bovine serum (FBS), 100 IU/mL penicillin, 100 μg mL^{-1} streptomycin and 1.4 mM L-Gloutamin, at 37°C, with 5% CO_2. All materials were provided by Costar and PAA. b) MTT assay: Cell growth inhibitory ability of the substances, expressed by the average IC_{50} value (substance's concentration required for 50% inhibition of cell growth), was analyzed using the MTT assay (3-(4,5-dimethylthiazol-2-yl)-2,5-diphenyltetrazolium bromide). Briefly, 3×10^3 A549 cells and 5×10^3 MRC-5 cells were cultured overnight on 96-well plates and culture media containing different concentrations (ranging from 1 to 850 μg mL^{-1}) of ADMA, Lap, Lap/ADMA, GO and GO/ADMA were added. All substances were dissolved in sterilized water (solvent). The 96-well plates with culture media containing different volumes of sterilized water (solvent), equal to volumes of solutions added to the test wells, were considered as control. After incubation for 48 h, 50 μL of MTT were added in each well from a stock solution (3 μg mL^{-1}), and incubated for additional 3 h. The yielded purple formazans were re-suspended in 200 μL of DMSO, using a multi-channel pipette. The solution was spectrophotometrically measured (540 nm, subtract background absorbance measured at 690 nm) using a microplate spectrophotometer (Multiskan Spectrum, Thermo Fisher Scientific, Waltham, USA). All the experiments were performed at least in triplicate. IC_{50} values were determined by the curve of percentage of inhibition versus dose.

Adsorption of Chlorophenols: a) Swelling of materials: 10 mg of GO or GO/ADMA were swelled for 20 h in methanol under stirring in glass vials. Then, distilled deionized water was added to a final MeOH:H_2O 70:30 (v/v). 10 mg of SWy-2 or SWy-2/ADMA were swelled for 20 h in distilled deionized water (pH = 4.5) under stirring in glass vials. After 20 h methanol was added so the final volume ratio MeOH: water = 70:30 (v/v). This methanol:H_2O mixture was chosen for both materials, since the goal of this experiment was to compare the performance of the clay and GO-based materials. b) Adsorption: The solutes used were 2,4,6-trichlorophenol (2,4,6-TCP) pentachlorophenol (PCP) and 2,4-dichlorophenol (2,4-DCP) purchased from Aldrich (purity 97%). Stock solutions of 0.8 mM 2,4-DCP, 2,4,6-TCP and PCP were prepared in MeOH: H_2O [70:30 v/v]. Adsorption experiments were performed in batch. 2,4-DCP, 2,4,6-TCP or PCP were added, at concentrations ranging between 7 μM and 70 μM, in 10 mg of swelled dispersions of the pristine and hybrid materials. The pH of the reaction mixture was adjusted using NaOH to pH = 5.3 for both 2,4-DCP and 2,4,6-TCP and pH = 4.5 for PCP to ensure the presence of protonated form of the phenols since the pK_a of 2,4-DCP is 6.79, the pK_a of 2,4,6-TCP is 6.23 and the pK_a of PCP is 4.7.[47] Screening experiments showed that the adsorption was completed in 90 minutes. Thus, our measurements were performed after 2 h of incubation to ensure adsorption equilibrium. Then the samples were centrifuged and UV-Vis spectra of supernatants were measured in quartz cuvettes 6Q, 1 × 1cm. Controls were run for chlorophenol solutions every 2 h with no solid material in the reaction mixture. The UV-Vis spectra were recorded using a Perkin-Elmer Lambda-35 double beam spectrometer. Quantification of the chlorophenols was done using the peaks at 280 nm for 2,4-DCP, at 290 nm for 2,4,6-TCP and at 210 nm for PCP (see Supporting Information).

Supporting Information

Supporting Information is available from the Wiley Online Library or from the author.

Acknowledgements

K. Spyrou, G. Potsi, and E. K. Diamanti contributed equally to this work. This research received financial support from the "Top Research School" program of the Zernike Institute for Advanced Materials under the Bonus Incentive Scheme (BIS) of the Netherlands' Ministry of Education, Science, and Culture, and from the Foundation for Fundamental Research on Matter (FOM), which is part of the Netherlands Organisation for Scientific Research (NWO). This research has been co-financed by the European Union (European Social Fund – ESF) and from Greek national funds through the Operational Program "Education and Lifelong Learning" of the National Strategic Reference Framework (NSRF) – Research Funding Program: THALES. Investing in knowledge society through the European Social Fund. X. Ke and G. Van Tendeloo acknowledge the European Research Council, ERC Grant No. 246791 – COUNTATOMS. The authors gratefully acknowledge the use of the XRD unit of the Laboratory Network at the University of Ioannina.

Received: March 26, 2014
Published online: July 19, 2014

[1] G. Ali Mansoori, in *Adv. Chem. Phys.* John Wiley & Sons, Inc., NJ, USA **2008**, pp. 207–258.
[2] a) G. C. McIntosh, M. Yoon, S. Berber, D. Tománek, *Phys. Rev. B* **2004**, *70*, 045401; b) R. C. Merkle, *Nanotechnology* **2000**, *11*, 89–99; c) R. Rawls, *Chem. Engin. News* **2002**, *80*, 13.
[3] S. I. Zones, Y. Nakagawa, G. S. Lee, C. Y. Chen, L. T. Yuen, *Micropor. Mesopor. Mater.* **1998**, *21*, 199–211.
[4] M. A. Meador, *Annu. Rev. Mater. Sci.* **1998**, *28*, 599–630.
[5] G. A. Mansoori, T. F. George, G. Zhang, L. Assoufid, *Molecular Building Blocks for Nanotechnology*, Spinger, New York, **2007**.
[6] H. Ramezani, G. A. Mansoori, *Topics Appl. Phys.* **2007**, *109*, 44–71.
[7] A. Orzeszko, R. Gralewska, B. J. Starościak, Z. Kazimierczuk, *Acta Biochim. Pol.* **2000**, *47*, 87–94.
[8] J. G. Hardman, L. E. Limbird, *The Pharmacological Basis of Therapeutics*, 10th ed., McGraw-Hill Book Co, New York **2001**.
[9] a) M. S. Whittingham, A. J. Jacobson, *Intercalation Chemistry*-Academic, New York **1982**; b) A. Vaccari, *Appl. Clay Sci.* **1999**, *14*, 161–198; c) M. Darder, M. Lopez-Blanco, P. Aranda, F. Leroux, E. Ruiz-Hitzky, *Chem. Mater.* **2005**, *17*, 1969–1977; d) J. D. Choi, G. M. Choi, *Sens. Actuat. B* **2000**, *69*, 120–126; e) L. L. Zhang, S. Y. Zhao, X. N. Tian, X. S. Zhao, *Langmuir* **2010**, *26*, 17624–17628; f) J. N. Coleman, M. Lotya, A. O'Neill, S. D. Bergin, P. J. King, U. Khan, K. Young, A. Gaucher, S. De, R. J. Smith, I. V. Shvets, S. K. Arora, G. Stanton, H.-Y. Kim, K. Lee, G. T. Kim, G. S. Duesberg, T. Hallam, J. J. Boland, J. J. Wang, J. F. Donegan, J. C. Grunlan, G. Moriarty, A. Shmeliov, R. J. Nicholls, J. M. Perkins, E. M. Grieveson, K. Theuwissen, D. W. McComb, P. D. Nellist, V. Nicolosi, *Science* **2011**, *331*, 568–571.
[10] a) T. Shichi, K. Takagi, *J. Photochem. Photobiol. C* **2000**, *1*, 113–130; b) D. Gournis, V. Georgakilas, M. A. Karakassides, T. Bakas, K. Kordatos, M. Prato, M. Fanti, F. Zerbetto, *J. Am. Chem. Soc.* **2004**, *126*, 8561–8568; c) D. Gournis, L. Jankovic, E. Maccallini, D. Benne, P. Rudolf, J. F. Colomer, C. Sooambar, V. Georgakilas, M. Prato, M. Fanti, F. Zerbetto, G. H. Sarova, D. M. Guldi, *J. Am. Chem. Soc.* **2006**, *128*, 6154–6163; d) B. K. G. Theng, *The Chemistry of Clay Organic Reactions*, Adam Hilger, London **1974**.
[11] a) T. J. Pinnavaia, *Science* **1983**, *220*, 365–371; b) J. Konta, *Appl. Clay Sci.* **1995**, *10*, 275–335; c) G. Lagaly, *Solid State Ionics* **1986**, *22*, 43–51.
[12] a) A. Cornelis, P. Laszlo, *NATO ASI Ser., Ser. C* **1986**, *165*, 213–228; b) J. A. Ballantine, *NATOASI Ser., Ser. C* **1986**, *165*, 197–212.

[13] a) V. Georgakilas, D. Gournis, A. B. Bourlinos, M. A. Karakassides, D. Petridis, *Chem.Eur. J.* **2003**, *9*, 3904–3908; b) V. Georgakilas, D. Gournis, D. Petridis, *Angew. Chem. Int. Ed.* **2001**, *40*, 4286–4288.
[14] a) J. T. Kloprogge, *J. Porous Mat.* **1998**, *5*, 5–41; b) A. Gil, L. M. Gandía, M. A. Vicente, *Catalysis Rev.* **2000**, *42*, 145–212; c) Y. Ma, W. Tong, H. Zhou,S. L. Suib, *Micropor. Mesopor. Mater.* **2000**, *37*, 243–252; d) K. Ohtsuka, *Chem. Mater.* **1997**, *9*, 2039–2050.
[15] a) M. Boufatit, H. Ait-Amar, W. R. Mc Whinnie, *Desalination* **2008**, *223*, 366–374; b) T. A. Wolfe, T. Demirel, E. R. Baumann, *Clay Clay Min.* **1985**, *33*, 301–311.
[16] a) C. Viseras, P. Cerezo, R. Sanchez, I. Salcedo, C. Aguzzi, *Appl. Clay Sci.* **2010**, *48*, 291–295; b) M. I. Carretero, *Appl. Clay Sci.* **2002**, *21*, 155–163.
[17] C. Aguzzi, P. Cerezo, C. Viseras, C. Caramella, *Appl. Clay Sci.* **2007**, *36*, 22–36.
[18] a) A. Lerf, H. He, M. Forster, J. Klinowski, *J. Phys. Chem. B* **1998**, *102*, 4477–4482; b) N. I. Kovtyukhova, *Chem. Mater.* **1999**, *11*, 771–778; c) N. I. Kovtyukhova, B. R. Martin, J. K. N. Mbindyo, P. A. Smith, B. Razavi, T. S. Mayer, T. E. Mallouk, *J. Phys. Chem. B* **2001**, *105*, 8762–8769.
[19] H. K. Jeong, M. Jin, E. J. Ra, K. Y. Sheem, G. H. Han, S. Arepalli, Y. H. Lee, *ACS Nano* **2010**, *4*, 1162–1166.
[20] P. K. Ang, S. Wang, Q. L. Bao, J. T. L. Thong, K. P. Loh, *ACS Nano* **2009**, *3*, 3587–3594.
[21] A. Kumar, A. L. M. Reddy, A. Mukherjee, M. Dubey, X. B. Zhan, N. Singh, L. Ci, W. E. Billups, J. Nagurny, G. Mital, P. M. Ajayan, *ACS Nano* **2011**, *5*, 4345–4349.
[22] W. Lv, D. M. Tang, Y. B. He, C. H. You, Z. Q. Shi, X. C. Chen, C. M. Chen, P. X. Hou, C. Liu, Q. H. Yan, *ACS Nano* **2009**, *3*, 3730–3736.
[23] a) Z. Liu, J. T. Robinson, X. Sun, H. Dai, *J. Am. Chem. Soc.* **2008**, *130*, 10876–10877; b) C.-H. Lu, C.-L. Zhu, J. Li, J.-J. Liu, X. Chen, H.-H. Yang, *Chem. Commun.* **2010**, *46*, 3116–3118; c) X. Sun, Z. Liu, K. Welsher, J. Robinson, A. Goodwin, S. Zaric, H. Dai, *Nano Res.* **2008**, *1*, 203–212; d) X. Yang, X. Zhang, Y. Ma, Y. Huang, Y. Wang, Y. Chen, *J. Mater. Chem.* **2009**, *19*, 2710–2714; e) W. Yang, K. R. Ratinac, S. P. Ringer, P. Thordarson, J. J. Gooding, F. Braet, *Angew. Chem.-Int. Ed.* **2010**, *49*, 2114–2138; f) L. Zhang, J. Xia, Q. Zhao, L. Liu, Z. Zhang, *Small* **2010**, *6*, 537–544.
[24] a) Y. Chang, S.-T. Yang, J.-H. Liu, E. Dong, Y. Wang, A. Cao, Y. Liu, H. Wang, *Toxicol. Lett.* **2011**, *200*, 201–210; b) K. Wang, J. Ruan, H. Song, J. Zhang,Y. Wo, S. Guo, D. Cui, *Nanoscale Res. Lett.* **2010**, *6*, 8.
[25] a) A. B. Bourlinos, D. Gournis, D. Petridis, T. Szabo, A. Szeri, I. Dekany, *Langmuir* **2003**, *19*, 6050–6055; b) R. Y. N. Gengler, A. Veligura, A. Enotiadis, E. K. Diamanti, D. Gournis, C. Jozsa, B. J. van Wees, P. Rudolf, *Small* **2010**, *6*, 35–39.
[26] D. R. Dreyer, S. Park, C. W. Bielawski, R. S. Ruoff, *Chem. Soc. Rev.* **2010**, *39*, 228–240.
[27] R. N. Tiwari, L. Chang, *J. Appl. Phys.* **2010**, *107*, 103305.
[28] I. Dekany, R. Kruger-Grasser, A. Weiss, *Colloid Polym. Sci.* **1998**, *276*, 570–576.
[29] a) A. G. Johnston, D. A. Leigh, A. Murphy, J. P. Smart, M. D. Deegan, *J. Am. Chem. Soc.* **1996**, *118*, 10662–10663; b) D. A. Leigh, A. Murphy, J. P. Smart, A. M. Z. Slawin, *Angew. Chem.-Int. Ed.* **1997**, *36*, 728–732; c) C. Seel, F. Vögtle, *Chem.-Eur. J.* **2000**, *6*, 21–24.
[30] a) M. A. Karakassides, D. Gournis, D. Petridis, *Clay Min.* **1999**, *34*, 429–438; b) M. A. Karakassides, D. Petridis, D. Gournis, *Clay Clay Min.* **1997**, *45*, 649–658.
[31] P. Stathi, K. Litina, D. Gournis, T. S. Giannopoulos, Y. Deligiannakis, *J. Colloid Interface Sci.* **2007**, *316*, 298–309.
[32] D. W. Lee, L. De Los Santos V, J. W. Seo, L. L. Felix, A. Bustamante, J. M. Cole, C. H. W. Barnes, *J. Phys. Chem. B* **2010**, *114*, 5723–5728.
[33] F. Tuinstra, J. L. Koenig, *J. Chem. Phys.* **1970**, *53*, 1126–1130.
[34] M. A. Pimenta, G. Dresselhaus, M. S. Dresselhaus, L. G. Cançado, A. Jorio, R. Saito, *Phys. Chem. Chem. Phys.* **2007**, *9*, 1276–1291.
[35] K. N. Kudin, B. Ozbas, H. C. Schniepp, R. K. Prud'homme, I. A. Aksay, R. Car, *Nano Lett.* **2008**, *8*, 36–41.
[36] a) M. Herrera-Alonso, A. A. Abdala, M. J. McAllister, I. A. Aksay, R. K. Prud'homme, *Langmuir* **2007**, *23*, 10644–10649; b) Y. Lin, A. M. Rao, B. Sadanadan, E. A. Kenik, Y. P. Sun, *J. Phys. Chem. B* **2002**, *106*, 1294–1298.
[37] E. Metwalli, D. Haines, O. Becker, S. Conzone, C. G. Pantano, *J. Colloid Interface Sci.* **2006**, *298*, 825–831.
[38] a) D. Gournis, L. Jankovic, E. Maccallini, D. Benne, P. Rudolf, J. F. Colomer, C. Sooambar, V. Georgakilas,M. Prato, M. Fanti, F. Zerbetto, G. H. Sarova, D. M. Guldi, *J. Am. Chem. Soc.* **2006**, *128*, 6154–6163; b) T. L. Barr, in *Practical Surface Analysis*, 2nd ed. (Eds: D. Briggs, M. P. Seah), John Wiley & Sons, Inc., Chinchester, UK **1990**.
[39] D. Gournis, A. E. Mantaka-Marketou, M. A. Karakassides, D. Petridis, *Phys. Chem. Miner.* **2001**, *28*, 285–290.
[40] a) S. P. Economopoulos, G. Rotas, Y. Miyata, H. Shinohara, N. Tagmatarchis, *ACS Nano* **2010**, *4*, 7499–7507; b) A. Enotiadis, K. Angjeli, N. Baldino, I. Nicotera, D. Gournis, *Small* **2012**, *8*, 3338–3349.
[41] J. K. Park, Y. B. Choy, J.-M. Oh, J. Y. Kim, S.-J. Hwang, J.-H. Choy, *Int. J. Pharm.* **2008**, *359*, 198–204.
[42] a) L. Staudenmaier, *Ber. Deut. Chem. Ges.* **1898**, *31*, 1481; b) D. V. Stergiou, E. K. Diamanti, D. Gournis, M. I. Prodromidis, *Electrochem. Commun.* **2010**, *12*, 1307–1309.
[43] D. Gournis, A. E. Mantaka-Marketou, M. A. Karakassides, D. Petridis, *Phys. Chem. Miner.* **2001**, *28*, 285–290.
[44] D. Gournis, A. Lappas, M. A. Karakassides, D. Tobbens, A. Moukarika, *Phys. Chem. Miner.* **2008**, *35*, 49–58.
[45] M. Lotya, Y. Hernandez, P. J. King, R. J. Smith, V. Nicolosi, L. S. Karlsson, F. M. Blighe, S. De, W. Zhiming, I. T. McGovern, G. S. Duesberg, J. N. Coleman, *J. Am. Chem. Soc.* **2009**, *131*, 3611–3620.
[46] T. Ebina, T. Iwasaki, A. Chatterjee, M. Katagiri, G. D. Stucky, *J. Phys. Chem. B* **1997**, *101*, 1125–1129.
[47] A. Ribeiro, M. H. Neves, M. F. Almeida, A. Alves, L. Santos, *J. Chromatogr. A* **2002**, *975*, 267–274.